11

Computing and Visualization in Science manuscript No.
(will be inserted by the editor)

Finite volume schemes for multidimensional hyperbolic systems based on the use of bicharacteristics

Mária Lukáčová-Medviďová

Arbeitsbereich Mathematik, Technische Universität Hamburg-Harburg, Schwarzenbergstraße 95, 21 073 Hamburg, Germany

Received: date / Revised version: date

Abstract. In this survey paper we present an overview on recent results for the bicharacteristics based finite volume schemes, the so-called finite volume evolution Galerkin (FVEG) schemes. These methods were proposed to solve multidimensional hyperbolic conservation laws. They combine the usually conflicting design objectives of using the conservation form and following the characteritics, or bicharacteritics. This is realized by combining the finite volume formulation with approximate evolution operators, which use bicharacteristics of multidimensional hyperbolic system. In this way all of the infinitely many directions of wave propagation are taken into account. The main goal of this paper is to study long-time behaviour of the FVEG schemes. We present several numerical experiments which confirm the fact that the FVEG methods are well-suited for long-time simulations.

Key words Multidimensional finite volume methods, Bicharacteristics, Hyperbolic systems, Wave equation, Euler equations

1 Introduction

In general numerical solution of trully multidimensional systems of conservation laws is a challenging task. The main reason is that even for small initial data we do not have existence and qualitative results for the solution of multidimensional Riemann problems. In principle, we have two finite volume approaches to overcome this fact. Firstly, the are the so-called central finite volume methods (FVM), which does not use the Riemann problem, see e.g. [4] and the references therein. However if no characteristic information is taken into account they may not provide a satisfactory resolution when small time steps are enforced by the stability condition. Note that for multidimensional problems the central schemes have the CFL stability restrictions strongly less than 1.

The second approach is based on a quasi-dimensional splitting and on the use of approximate solution to the one-dimensional Riemann problem, which structure is well-understood. If main features, that we want to approximate are just one-dimensional, this approach can produce good qualitative results. But for complex genuinely multidimensional structures, such as oblique shocks or circular expansions, dimensional splitting approach can yield spurious local wave structure resolutions. Looking back to the literature of the last decade we find several new genuinely multidimensional methods. For example, the wave propagation algorithm of LeVeque [5], the method of transport (MoT) of Fey [3] and its simplified version of Noelle [17], or the multistate FVM of Brio et al. [2]. The latter approach is based on the use of the Kirchoff formulae for the wave equation or the linearized Euler equations in order to correct multidimensional contributions in corners of the computational cells. In fact, our approach is similar to that of Brio. However, instead of the Kirchhoff formulae which are explicit in time but singular over the sonic circle, we use a different method. We work with a general theory of bicharacteristics for linear hyperbolic systems of first order and derive the so-called approximate evolution operators. This is the most involved part of the derivation of our schemes.

The basic idea of the *evolution Galerkin schemes (EG)*, introduced by Morton, see e.g. [15], is the following. Transport quantities are shifted along characteristics and then projected onto a finite element space. Following the work of Ostkamp [18] we have derived in [7] several new evolution Galerkin methods for the linear system of the wave equation, which have better stability properties as well as global accuracy. Their generalization to the second order EG method was done in [11] for linear two-dimensional systems. In [6] we have studied the two-dimensional Riemann problem for the wave equation system and demonstrated good accuracy of the EG schemes as well as correct multidimensional resolution of oblique shocks.

⋆ This research was supported by the Volkswagen-Stiftung

In their dissertation [19] Ostkamp proposed a generalization of the EG method to the nonlinear Euler equations. However, in order to implement her scheme quite tedious calculations of three-dimensional integrals had to be done. It was barely feasible for practical applications, such as the shallow water equations and the Euler equations, especially for higher order methods. The decisive step was to take a different approach, which yield us to the finite volume framework. In the so-called *finite volume evolution Galerkin (FVEG)* methods the approximate evolutions are used only on cell interfaces to evaluate the numerical fluxes.

Note that there is a connection between the FVEG method and the interface centered MoT of Noelle. Both methods use multidimensional evolution only on cell-interfaces instead of on whole computational cells. This leads to the crucial simplification of original methods within the FV framework.

The *aim of this paper* is to give a self-contained introductory overview on the recent results of the evolution Galerkin schemes. We want to present basic ideas of the theory of bicharacteristics, which are used for the derivation of exact and approximate evolution operators for general multidimensional hyperbolic systems. We illustrate the application of these techniques on the Euler equations system. Further interesting applications are, for example, the wave equation system, the shallow water equations, the magneto-hydrodynamic equations or the equations of nonlinear elasticity. In the last section the long-time behaviour of the FVEG schemes is studied. We present new numerical results confirming that the schemes are well-suited for long-time simulations.

The paper is organized as follows. In Section 2 the exact integral representation for the linearized Euler equations are presented. Approximation of the so-called mantle integrals is discussed in Section 3. We describe the EG3 approximate evolution operator [7] and following the lines of our recent paper [10] present new approximate evolution operators, which yield numerical schemes stable up to the CFL number 1. The formulation of the finite volume evolution Galerkin scheme is given in Section 4. Second order resolution is obtained by means of a bilinear recovery in space and the midpoint rule approximation in time. In order to apply the approximate evolution operator to fully nonlinear systems, such as the Euler equations of gas dynamics or the shallow water equations, first a suitable linearization is needed. It is done by freezing the Jacobian matrices locally around suitable constant states. Despite the linearization procedure the FVEG methods authomatic satisfy the entropy condition on sonic rarefaction waves and no entropy fix is needed, see [9], [10] for numerical experiments.

The error analysis of the FVEG methods was presented in [10]. For linear or linearized systems it was proved that if a bilinear recovery is used the method is of second order in space and time. In Section 5 we show through numerical expeiments that the constant of the leading error is considerably smaller in comparison to other commonly used methods. This leads us to the conclusion that the FVEG methods are well-suited for long-time simulations, which will be confirmed by several numerical experiments.

2 Linerized Euler equations and evolution operator

In order to derive an evolution operator for the Euler equations it is suitable to work with this system in primitive variables

$$\boldsymbol{v}_t + \boldsymbol{A}_1(\boldsymbol{v})\boldsymbol{v}_x + \boldsymbol{A}_2(\boldsymbol{v})\boldsymbol{v}_y = 0, \quad \boldsymbol{x} = (x,y)^T, \qquad (1)$$

where $\boldsymbol{v} := (\rho, u, v, p)^T$ is the vector of primitive variables and the Jacobian matrices are given by

$$\boldsymbol{A}_1 := \begin{pmatrix} u & \rho & 0 & 0 \\ 0 & u & 0 & \frac{1}{\rho} \\ 0 & 0 & u & 0 \\ 0 & \gamma p & 0 & u \end{pmatrix}, \quad \boldsymbol{A}_2 := \begin{pmatrix} v & 0 & \rho & 0 \\ 0 & v & 0 & 0 \\ 0 & 0 & v & \frac{1}{\rho} \\ 0 & 0 & \gamma p & v \end{pmatrix}.$$

Here ρ denotes the density, u and v components of velocity, p pressure and γ isentropic exponent; $\gamma = 1.4$ for dry air. In what follows we briefly describe main technique for deriving an integral representation (or an exact evolution operator). First, we linearise system (1) by freezing the Jacobian matrices at a suitable point $\tilde{P} = (\tilde{x}, \tilde{y}, \tilde{t})$. Denote by $\tilde{\boldsymbol{v}} = (\tilde{\rho}, \tilde{u}, \tilde{v}, \tilde{p})$ the local variables at the point $\tilde{P}$ and by $\tilde{c}$ the local speed of sound there, i.e. $\tilde{c} = \sqrt{\frac{\gamma\tilde{p}}{\tilde{\rho}}}$. Thus, the linearised system (1) with frozen constant coefficient matrices has the form

$$\boldsymbol{v}_t + \boldsymbol{A}_1(\tilde{\boldsymbol{v}})\boldsymbol{v}_x + \boldsymbol{A}_2(\tilde{\boldsymbol{v}})\boldsymbol{v}_y = 0, \quad \boldsymbol{x} = (x,y)^T. \qquad (2)$$

The eigenvalues of the matrix pencil $\boldsymbol{A}(\tilde{\boldsymbol{v}}) = \boldsymbol{A}_1(\tilde{\boldsymbol{v}})n_x + \boldsymbol{A}_2(\tilde{\boldsymbol{v}})n_y$, where $\boldsymbol{n} = \boldsymbol{n}(\theta) = (n_x, n_y)^T = (\cos\theta, \sin\theta)^T \in \mathbb{R}^2$ are

$$\begin{aligned} \lambda_1 &= \tilde{u}\cos\theta + \tilde{v}\sin\theta - \tilde{c}, \\ \lambda_2 &= \lambda_3 = \tilde{u}\cos\theta + \tilde{v}\sin\theta, \\ \lambda_4 &= \tilde{u}\cos\theta + \tilde{v}\sin\theta + \tilde{c}, \end{aligned}$$

and the corresponding linearly independent right eigenvectors are

$$\begin{aligned} \boldsymbol{r}_1 &= \left(-\frac{\tilde{\rho}}{\tilde{c}}, \cos\theta, \sin\theta, -\tilde{\rho}\tilde{c}\right)^T, \\ \boldsymbol{r}_2 &= (1,0,0,0)^T, \\ \boldsymbol{r}_3 &= (0, \sin\theta, -\cos\theta, 0)^T, \\ \boldsymbol{r}_4 &= \left(\frac{\tilde{\rho}}{\tilde{c}}, \cos\theta, \sin\theta, \tilde{\rho}\tilde{c}\right)^T. \end{aligned}$$

Let $\boldsymbol{R}(\tilde{\boldsymbol{v}})$ be the matrix of the right eigenvectors and $\boldsymbol{R}^{-1}(\tilde{\boldsymbol{v}})$ its inverse. Denote by $\boldsymbol{w}$ the vector of characteristic variables

$$\boldsymbol{w} = \boldsymbol{R}^{-1}(\tilde{\boldsymbol{v}})\boldsymbol{v} = \begin{pmatrix} \frac{1}{2}(-\frac{p}{\tilde{\rho}\tilde{c}} + u\cos\theta + v\sin\theta) \\ \rho - \frac{p}{\tilde{c}^2} \\ u\sin\theta - v\cos\theta \\ \frac{1}{2}(\frac{p}{\tilde{\rho}\tilde{c}} + u\cos\theta + v\sin\theta) \end{pmatrix}.$$

Multiplying system (2) by $\boldsymbol{R}^{-1}(\tilde{\boldsymbol{v}})$ from the left we obtain the following system written in characteristic variables

$$\boldsymbol{w}_t + \boldsymbol{B}_1(\tilde{\boldsymbol{v}})\boldsymbol{w}_x + \boldsymbol{B}_2(\tilde{\boldsymbol{v}})\boldsymbol{w}_y = 0, \tag{3}$$

where $\boldsymbol{B}_1$, $\boldsymbol{B}_2$ are transformed Jacobian matrices. Being in one space dimension the system (3) reduces to a diagonal system consisting of separated advection equations. Their exact evolution operator reads

$$w_\ell(x,t) = w_\ell(x - \lambda_\ell t, 0), \qquad \ell = 1,\dots,4. \tag{4}$$

In the multidimensional case the system (3) will reduce to a diagonal one only if the Jacobian matrices $\boldsymbol{A}_1$, $\boldsymbol{A}_2$ commute, which is not the case of the two-dimensional Euler equations. We rewrite the system (3) in the form of the following quasi-diagonalised system

$$\boldsymbol{w}_t + \begin{pmatrix} \tilde{u}-\tilde{c}\cos\theta & 0 & 0 & 0 \\ 0 & \tilde{u} & 0 & 0 \\ 0 & 0 & \tilde{u} & 0 \\ 0 & 0 & 0 & \tilde{u}+\tilde{c}\cos\theta \end{pmatrix} \boldsymbol{w}_x + \begin{pmatrix} \tilde{v}-\tilde{c}\sin\theta & 0 & 0 & 0 \\ 0 & \tilde{v} & 0 & 0 \\ 0 & 0 & \tilde{v} & 0 \\ 0 & 0 & 0 & \tilde{v}+\tilde{c}\sin\theta \end{pmatrix} \boldsymbol{w}_y = \boldsymbol{S} \tag{5}$$

with

$$\boldsymbol{S} = \begin{pmatrix} \frac{1}{2}\tilde{c}(\sin\theta\frac{\partial w_3}{\partial x} - \cos\theta\frac{\partial w_3}{\partial y}) \\ 0 \\ \tilde{c}\sin\theta(\frac{\partial w_1}{\partial x} - \frac{\partial w_4}{\partial x}) - \tilde{c}\cos\theta(\frac{\partial w_1}{\partial y} - \frac{\partial w_4}{\partial y}) \\ \frac{1}{2}\tilde{c}(-\sin\theta\frac{\partial w_3}{\partial x} + \cos\theta\frac{\partial w_3}{\partial y}) \end{pmatrix}.$$

Each characteristic variable w_ℓ, $\ell = 1,\dots,4$, is evolved in time along the corresponding bicharacteristic curve x_ℓ defined by

$$\frac{\mathrm{d}\boldsymbol{x}_\ell}{\mathrm{d}t} = \boldsymbol{b}_{\ell\ell}(\boldsymbol{n}) := (b^1_{\ell\ell}, b^2_{\ell\ell})^T, \tag{6}$$

where $\boldsymbol{B}_1 = (b^1_{jk})_{1\le j,k\le 4}$, $\boldsymbol{B}_2 = (b^2_{jk})_{1\le j,k\le 4}$. The set of all bicharacteristics creates a mantle of the so-called Mach cone, see Fig. 1. In order to obtain the exact evolution of each characteristic variable w_ℓ we integrate the ℓ-th equation of the system (5) from the apex $P = (x, y, t+\Delta t)$ down to the corresponding footpoint $Q_\ell(\theta)$:

$$\begin{aligned} Q_1(\theta) &= (x - (\tilde{u} - \tilde{c}\cos\theta)\Delta t, y - (\tilde{v} - \tilde{c}\sin\theta)\Delta t, t), \\ Q_2 = Q_3 &= (x - \tilde{u}\triangle t, y - \tilde{v}\Delta t, t), \\ Q_4(\theta) &= (x - (\tilde{u} + \tilde{c}\cos\theta)\Delta t, y - (\tilde{v} + \tilde{c}\sin\theta)\Delta t, t). \end{aligned}$$

Multiplying the resulting system from the left by the matrix $\boldsymbol{R}$ yields the exact integral equations for the original primitive variables.

$$\rho(P) = \rho(Q_2) - \frac{p(Q_2)}{\tilde{c}^2} + \frac{1}{2\pi}\int_0^{2\pi}\Big[\frac{p(Q_1)}{\tilde{c}^2} - \frac{\tilde{\rho}}{\tilde{c}}u(Q_1)\cos\theta - \frac{\tilde{\rho}}{\tilde{c}}v(Q_1)\sin\theta\Big]\mathrm{d}\theta$$

$$-\frac{\tilde{\rho}}{\tilde{c}}\frac{1}{2\pi}\int_0^{2\pi}\int_t^{t+\triangle t} S(\boldsymbol{\xi},\tilde{t},\theta)\mathrm{d}\tilde{t}\mathrm{d}\theta, \tag{7}$$

$$u(P) = \frac{1}{2\pi}\int_0^{2\pi}\Big[-\frac{p(Q_1)}{\tilde{\rho}\tilde{c}}\cos\theta + u(Q_1)\,\cos^2\theta + v(Q_1)\sin\theta\cos\theta\Big]\mathrm{d}\theta$$

$$+\frac{1}{2\pi}\int_0^{2\pi}\int_t^{t+\triangle t}\cos\theta\, S(\boldsymbol{\xi},\tilde{t},\theta)\mathrm{d}\tilde{t}\mathrm{d}\theta$$

$$+\frac{1}{2}u(Q_2) - \frac{1}{2\tilde{\rho}}\int_t^{t+\triangle t} p_x(Q_2(\tilde{t}))\mathrm{d}\tilde{t}, \tag{8}$$

$$v(P) = \frac{1}{2\pi}\int_0^{2\pi}\Big[-\frac{p(Q_1)}{\tilde{\rho}\tilde{c}}\sin\theta + u(Q_1)\cos\theta\sin\theta + v(Q_1)\sin^2\theta\Big]\mathrm{d}\theta$$

$$+\frac{1}{2\pi}\int_0^{2\pi}\int_t^{t+\triangle t}\sin\theta S(\boldsymbol{\xi},\tilde{t},\theta)\mathrm{d}\tilde{t}\mathrm{d}\theta$$

$$+\frac{1}{2}v(Q_2) - \frac{1}{2\tilde{\rho}}\int_t^{t+\triangle t} p_y(Q_2(\tilde{t}))\mathrm{d}\tilde{t}, \tag{9}$$

$$p(P) = \frac{1}{2\pi}\int_0^{2\pi}[p(Q_1) - \tilde{\rho}\tilde{c}u(Q_1)\cos\theta - \tilde{\rho}\tilde{c}v(Q_1)\sin\theta]\mathrm{d}\theta$$

$$-\tilde{\rho}\tilde{c}\frac{1}{2\pi}\int_0^{2\pi}\int_t^{t+\triangle t} S(\boldsymbol{\xi},\tilde{t},\theta)\,\mathrm{d}\tilde{t}\mathrm{d}\theta, \tag{10}$$

where $\boldsymbol{\xi} = (\boldsymbol{x} - (\tilde{\boldsymbol{u}} - \tilde{c}\boldsymbol{n}(\theta))(t+\triangle t - \tilde{t})) = (x - (\tilde{u} - \tilde{c}\cos\theta)(t+\triangle t - \tilde{t}), y - (\tilde{v} - \tilde{c}\sin\theta)(t+\triangle t - \tilde{t}))$, and the so-called source term S is given in the following form

$$S(\boldsymbol{x},t,\theta) := \tilde{c}[u_x(\boldsymbol{x},t,\theta)\sin^2\theta - (u_y(\boldsymbol{x},t,\theta)$$

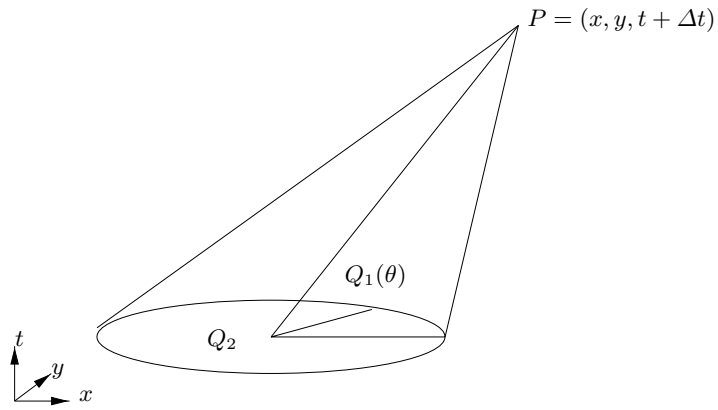

Fig. 1. Bicharacterestics along the Mach cone through P and $Q_\ell(\theta)$.

$$+ v_x(\boldsymbol{x},t,\theta))\sin\theta\cos\theta + v_y(\boldsymbol{x},t,\theta)\cos^2\theta].$$

3 Approximate evolution operators

Note that the above exact integral representation (7)-(10) is implicit in time. In order to derive a numerical scheme, which is explicit in time, time integrals of the source term, the so-called *mantle integrals*, have to be approximated with suitable numerical quadratures. In this way several approximate evolution operators were derived and evaluated with respect to its accuracy and stability, see [7]. We have shown in [7] that the rectangle rule in time in the source term leads an approximate evolution operator, the so-called EG3 operator, whose accuracy is the best among other approximate operators obtained by the "classical" numerical quadratures. See [7] for the EG1, EG2 operators and [20] for the EG4 approximate operator.
In what follows we write equations for approximate evolution of ρ, u, p; the approximate evolution operator for v is analogous to that of u.

3.1 Approximate evolution operator EG3

$$\rho(P) = \rho(Q_2) + \frac{1}{2\pi}\int_0^{2\pi}\Big[\frac{\rho(Q_1)}{\gamma} - 2\frac{\tilde\rho}{\tilde c}\left(u(Q_1)\cos\theta + v(Q_1)\sin\theta\right)\Big]\mathrm{d}\theta + \mathcal{O}(\Delta t^2), \quad (11)$$

$$u(P) = \frac{1}{2}u(Q_2) + \frac{1}{2\pi}\int_0^{2\pi}\Big[-\frac{p(Q_1)}{\tilde\rho\tilde c}\cos\theta + u(Q_1)\left(3\cos^2\theta - 1\right) + 3v(Q_1)\sin\theta\cos\theta\Big]\mathrm{d}\theta + \mathcal{O}(\Delta t^2), \quad (12)$$

$$p(P) = \frac{1}{2\pi}\int_0^{2\pi}[p(Q_1) - 2\tilde\rho\tilde c(u(Q_1)\cos\theta + v(Q_1)\sin\theta)]\mathrm{d}\theta + \mathcal{O}(\Delta t^2). \quad (13)$$

Our numerical experiments for the wave equation system demonstrate that the second order FVEG3 scheme is 7 times more accurate than the commonly used numerical scheme, e.g. the Lax-Wendroff scheme (rotated Richtmyer version), the wave propagation algorithm of LeVeque [5], quasi-dimensional splitting finite volume schemes; see [8].
On the other hand the above FVEG methods suffered from the restrictive stability limits. For example, for the FVEG3 scheme a typical CFL stability limit was 0.63 and 0.56 for first and second order schemes, respectively. Note that integrals around the sonic circle, i.e. $\int_0^{2\pi}\mathrm{d}\theta$, are evaluated for the piecewise constant data or piecewise bilinear ansatz data exactly. Therefore, obviously the only step where the stability could be reduced was the time approximation of the mantle integral. For example, in the first order EG scheme we work with piecewise constant data, in which case a discontinuity cuts through the cone mantle. Naturally, classical quadratures, such as the rectangle or the trapezoidal rule, which were used for the EG1 - EG4 schemes, cannot correctly reproduce integration of discontinous data.
From one-dimensional advection on a uniform mesh we know that any scheme that is stable for CFL numbers up to 1 reproduces the exact solution to the advection problems, i.e. the data shifted by one mesh cell for CFL= 1, cf. (4) for the exact evolution operator. In our forthcomming paper [10] we look for the approximate evolution operators by postulating the following design principle. Each one-dimensional planar wave propagating in $x-$ or $y-$ direction has to be reproduced exactly by the approximate evolution operator. Thus, we consider piecewise constant or piecewise bilinear ansatz data in order to derive corresponding approximate evolution operators for the first or second order FVEG schemes, respectively. See [10] for a detailed derivation as well as for numerical experiments, which demonstrate the full stability up to CFL=1.

3.2 Approximate evolution operator E_Δ^{const} for piecewise constant data

$$\rho(P) = (1-\frac{1}{\gamma})\rho(Q_2) + \frac{1}{2\pi}\int_0^{2\pi}\Big[\frac{\rho(Q_1)}{\gamma} - \frac{\tilde\rho}{\tilde c}\left(u(Q_1)\mathrm{sgn}(\cos\theta) + v(Q_1)\mathrm{sgn}(\sin\theta)\right)\Big]\mathrm{d}\theta + \mathcal{O}(\Delta t^2), \quad (14)$$

$$u(P) = \frac{1}{2\pi}\int_0^{2\pi}\Big[-\frac{p(Q_1)}{\tilde\rho\tilde c}\mathrm{sgn}(\cos\theta) + u(Q_1)\left(\tfrac{1}{2} + \cos^2\theta\right) + v(Q_1)\sin\theta\cos\theta\Big]\mathrm{d}\theta + \mathcal{O}(\Delta t^2), \quad (15)$$

$$p(P) = \frac{1}{2\pi}\int_0^{2\pi}[p(Q_1) - \tilde\rho\tilde c(u(Q_1)\mathrm{sgn}(\cos\theta) + v(Q_1)\mathrm{sgn}(\sin\theta))]\mathrm{d}\theta + \mathcal{O}(\Delta t^2). \quad (16)$$

3.3 Approximate evolution operator E_Δ^{bilin} for piecewise bilinear data

$$\rho(P) = \rho(Q_2) + \frac{1}{4}\int_0^{2\pi}\frac{1}{\gamma}\left[\rho(Q_1) - \rho(Q_2)\right]\mathrm{d}\theta - \frac{1}{\pi}\int_0^{2\pi}\frac{\tilde\rho}{\tilde c}\left[u(Q_1)\cos\theta + v(Q_1)\sin\theta\right]\mathrm{d}\theta + \mathcal{O}(\Delta t^2), \quad (17)$$

$$u(P) = u(Q_2) - \frac{1}{\pi}\int_0^{2\pi} \frac{p(Q_1)}{\tilde{\rho}\tilde{c}} \cos\theta \mathrm{d}\theta + \frac{1}{4}\int_0^{2\pi} \Big[3(u(Q_1)\cos\theta + v(Q_1)\sin\theta)\cos\theta - u(Q_1) - \tfrac{1}{2}u(Q_2)\Big]\mathrm{d}\theta + \mathcal{O}(\Delta t^2), \quad (18)$$

$$p(P) = p(Q_2) + \frac{1}{4}\int_0^{2\pi} [p(Q_1) - p(Q_2)]\,\mathrm{d}\theta - \frac{1}{\pi}\int_0^{2\pi} \bar{\rho}\bar{a}\,[u(Q_1)\cos\theta + v(Q_1)\sin\theta]\,\mathrm{d}\theta + \mathcal{O}(\Delta t^2). \quad (19)$$

4 Finite volume evolution Galerkin method

Let Ω be our two-dimensional computational domain covered by the regular square mesh cells

$$\Omega_{ij} \equiv [(i-\tfrac{1}{2})h, (i+\tfrac{1}{2})h] \times [(j-\tfrac{1}{2})h, (j+\tfrac{1}{2})h] = [x_{i-1/2}, x_{i+1/2}] \times [y_{j-1/2}, y_{j+1/2}],$$

where $i, j \in \mathbb{Z}$, and $h > 0$ is the mesh size parameter.

In finite volume schemes typically the one-dimensional Riemann problems in the normal direction to cell interfaces are used to approximate fluxes on cell interfaces. Instead of this dimensional-splitting technique we use in our scheme a genuinely multidimensional approach. In order to compute fluxes on cell interfaces the value of $\boldsymbol{U}$ will be determined by means of a suitable approximate evolution operator. In this way all directions of wave propagation are explicitly taken into account.

Consider the Euler equations written in the conservative variables

$$\boldsymbol{u}_t + \boldsymbol{f}_1(\boldsymbol{u})_x + \boldsymbol{f}_2(\boldsymbol{u})_y = 0, \quad (20)$$

where the vector of conservative variables is $\boldsymbol{u} := (\rho, \rho u, \rho v, e)^T$ and the fluxes are

$$\boldsymbol{f}_1(\boldsymbol{u}) := \begin{pmatrix} \rho u \\ \rho u^2 + p \\ \rho uv \\ (e+p)u \end{pmatrix}, \quad \boldsymbol{f}_2(\boldsymbol{u}) := \begin{pmatrix} \rho v \\ \rho uv \\ \rho v^2 + p \\ (e+p)v \end{pmatrix}.$$

Here e stands for the total energy, i.e. $e = p/(\gamma - 1) + \rho(u^2 + v^2)/2$.

Let us integrate (20) over a mesh cell Ω_{ij} and time interval $[t_n, t_{n+1}]$. Applying the Gauss theorem for the flux integrals and rewriting the cell volume integrals by the cell interface integrals yield the finite volume formulation. The crucial point of the FVEG schemes is the use of the approximate evolution operators for the evaluation of fluxes at cell interfaces.

The time integral of fluxes is approximated by the midpoint rule. If no recovery is used the whole method is of first order. In this case the finite volume evolution Galerkin scheme reads

$$\boldsymbol{U}^{n+1} = \boldsymbol{U}^n - \frac{\Delta t}{h}\sum_{k=1}^{2} \delta_{x_k} \boldsymbol{f}_k(\boldsymbol{U}^{n+1/2}), \quad (21)$$

$$\boldsymbol{f}_k(\boldsymbol{U}^{n+1/2}) = \frac{1}{h}\int_{\mathcal{E}} \boldsymbol{f}_k(E_{\Delta t/2}\boldsymbol{U}^n)\mathrm{d}S, \quad (22)$$

where $\delta_{x_k}\boldsymbol{f}_k(\boldsymbol{U}^{n+1/2})$ represents an approximation to the edge flux difference at the intermediate time level $t_n + \Delta t/2$. The cell interface fluxes $\boldsymbol{f}_k(\boldsymbol{U}^{n+1/2})$, are evolved using an approximate evolution operator denoted by $E_{\Delta t/2}$ to $t_n + \Delta t/2$ and averaged along the cell interface $\mathcal{E}$.

It is possible to define a second order FVEG scheme just by using the first order approximate evolution operators E_Δ^{bilin} (17) - (19) or the operator EG3 (11) - (13) and discontinuous conservative bilinear recovery. In fact, in such a way the second order FVEG3 scheme was constructed in [12]. However, our experience from [10] shows that the desirable scheme, i.e. the best stability range as well as the best accuracy, is the scheme, which is given by a suitable combination of E_Δ^{const} and E_Δ^{bilin}. We use E_Δ^{bilin} to evolve slopes and E_Δ^{const} to evolve the corresponding constant part:

$$\boldsymbol{f}_k(\boldsymbol{U}^{n+1/2}) = \frac{1}{h}\int_{\mathcal{E}} \boldsymbol{f}_k\Big(E_\Delta^{bilin} R_h \boldsymbol{U}^n + E_\Delta^{const}(1 - \mu_x^2\mu_y^2)\boldsymbol{U}^n\Big)\mathrm{d}S. \quad (23)$$

where $\mu_x^2 U_{ij} = 1/4(U_{i+1,j} + 2U_{ij} + U_{i-1,j})$; an analogous notation is used for the $y-$direction.

Here R_h denotes the continuous bilinear recovery, the so-called isoparametric bilinear approximation. Each vertex value is obtained as a mean of the cell averages from all the cells that share the vertex. Unfortunately such a recovery does not preserve the cell averages, which leads to reduced total accuracy of the scheme, see [10] for numerical experiments and [1], [16] for further arguments. Therefore our aim is to recover conservation over cells, i.e. to construct such a reconstructed approximation $\tilde{\boldsymbol{U}}$ that the following property holds

$$\int_{\Omega_{ij}} \tilde{\boldsymbol{U}}\mathrm{d}\boldsymbol{x} = \int_{\Omega_{ij}} \boldsymbol{U}\mathrm{d}\boldsymbol{x}.$$

This can be done by changing the constant part of the approximate function, so that we have on each cell Ω_{ij}, $i, j, \in \mathbb{Z}$

$$\tilde{\boldsymbol{U}} = R_h\boldsymbol{U} + (1 - \mu_x^2\mu_y^2)\boldsymbol{U}.$$

This is now conservative and discontinuous across cell boundary.

In order to compute fluxes on cell interfaces by means of (22) or (23) double integrals along the cell interface and around the Mach cone $\int_{\mathcal{E}}\int_0^{2\pi} \mathrm{d}\theta\mathrm{d}S$ have to be computed. Since our goal is to take all infinitely many directions of wave propagation into account, integrals around the Mach cone will be evaluated exactly. This can be done for any basis function, such as 1, x, y, xy, $x\cos\theta$, $x\sin\theta$, $x\sin\theta\cos\theta$, etc., which are defined on each Ω_{ij}, $i, j, \in \mathbb{Z}$. The results of exact integration yield new weights in finite difference stencils, which correspond to the approximate evolution operators.

In order to simplify the derivation and implementation of the second order scheme for the Euler equations we approximate cell interface integrals by Simpson's rule and evaluate fluxes at vertices and midpoints. They are these points $\tilde{P}$ where the linearization of the nonlinear Euler equations is done. The local flow information $\tilde{u}, \tilde{v}, \tilde{a}$ are computed by an averaging process; we average over four cells adjacent to the vertex or over two cells adjacent to the midpoints.

The approach described above can be generalized to the third order FVEG schemes, see [13] for more details. In [14], [20] implementations of different boundary conditions are studied.

5 Numerical experiments

In this section, through long-time numerical simulations, we illustrate the performance of the FVEG method for the linear wave equation system, see [10] for its approximate evolution operators, and for fully nonlinear Euler equations of gas dynamics.

5.1 Comparison of global accuracy for long-time simulations

First we present comparison of global accuracy of the second order FVEG scheme (21), (23), the second order FVEG3 scheme and other commonly used numerical schemes for approximation of hyperbolic conservation laws. As an example we have chosen the Lax-Wendroff (LW) scheme (rotated Richtmyer version) and the wave propagation algorithm of LeVeque (the second order $\mathrm{T}^{2,2}$ version) [5]. Consider the initial value problem for the wave equation system

$$\begin{aligned} \phi_t + c(u_x + v_y) &= 0 \\ u_t + c\phi_x &= 0 \\ v_t + c\phi_y &= 0 \end{aligned} \tag{24}$$

with the initial data

$$\begin{aligned} \phi(\boldsymbol{x}, 0) &= -\frac{1}{c}(\sin 2\pi x + \sin 2\pi y), \\ u(\boldsymbol{x}, 0) &= 0 = v(\boldsymbol{x}, 0). \end{aligned}$$

In this case the exact solution is known

$$\begin{aligned} \phi(\boldsymbol{x}, t) &= -\frac{1}{c}\cos 2\pi ct(\sin 2\pi x + \sin 2\pi y), \\ u(\boldsymbol{x}, t) &= \frac{1}{c}\sin 2\pi ct \cos 2\pi x, \\ v(\boldsymbol{x}, t) &= \frac{1}{c}\sin 2\pi ct \cos 2\pi y. \end{aligned}$$

In the following table we compare the accuracy of the above schemes for long-time simulations and take an end time $T = 10$. The CFL number is taken to be $\nu \equiv c\Delta t/h = 0.9$ for the FVEG scheme (21), (23), the Lax-Wendroff scheme and the LeVeque $\mathrm{T}^{2,2}$ scheme. For computations with the FVEG3 scheme we can only use smaller CFL number, say $\nu = 0.55$, due to its reduced stability range.
Note that due to zero advection velocity $\tilde{u} = \tilde{v} = 0$ we can approximate the cell interface integrals in both FVEG schemes by the trapezoidal rule, which generally leads to a stable scheme if $\tilde{u} = \tilde{v}$.
We present the L^2- errors for meshes of 20×20, $40 \times 40, \ldots, 160 \times 160$ cells, together with the experimental order of convergence (EOC) computed from two meshes of sizes $N_1 \times N_1$ and $N_2 \times N_2$ as

$$\mathrm{EOC} = \ln \frac{\|\boldsymbol{u}_{N_1}(T) - \boldsymbol{U}^n_{N_1}\|}{\|\boldsymbol{u}_{N_2}(T) - \boldsymbol{U}^n_{N_2}\|} / \ln\left(\frac{N_2}{N_1}\right).$$

Here we have denoted by $\boldsymbol{u}_N(T)$ and by $\boldsymbol{U}^n_N$ the exact and the approximate solutions on a mesh of size $N \times N$, respectively.

Table 1. Accuracy of the FVEG schemes, the Lax-Wendroff scheme and the $\mathrm{T}^{2,2}$ scheme for long-time simulations.

$\|\boldsymbol{u}(T) - \boldsymbol{U}^n\|/N$	FVEG	FVEG3	LW	$\mathrm{T}^{2,2}$
20	0.386944	1.419723	1.294829	1.294829
40	0.087802	0.335918	0.383314	0.383314
80	0.021017	0.062675	0.098100	0.098099
160	0.005196	0.013484	0.024551	0.024550
EOC	2.01608	2.21664	1.99847	1.99852

The global L^2-error of the FVEG scheme is almost 5 times smaller than the error of the Lax-Wedroff scheme and the LeVeque wave propagation algorithm. These results demonstrate that the constant of the leading order error of the FVEG scheme is also for long-time simulations considerably smaller than that of other commonly used schemes. Note also that the new FVEG scheme (21), (23) has not only better stability but it has also higher global accuracy than the FVEG3 scheme, which is due to reduced number of projection steps. In fact the L^2- error of the FVEG scheme (21), (23) is 2.5 times smaller than the error of the FVEG3 scheme. It should be also pointed out that generally the CPU costs for the FVEG scheme and the LeVeque scheme are comparable.

5.2 Water waves propagation

It is known that the approximation of circular waves on rectangular meshes can cause difficulties. Particularly, if the dimensional splitting approach is used the spurious mesh oriented structures can be developed, see e.g. [5], [7], [17] and the references therein.
We consider the wave equation system (24) with the following initial data modelling a pointwise disturbance

$$\begin{aligned} \phi(\boldsymbol{x}, 0) &= -c\exp(-15x^2 - 15y^2), \\ u(\boldsymbol{x}, 0) &= 0 = v(\boldsymbol{x}, 0). \end{aligned}$$

The computational domain $[-3,3]\times[-3,3]$ is divided into 100×100 cells. The solution obtained by the second order FVEG scheme at different times from $T=0.2$ until $T=8.0$ is shown in Figures 2 - 4. We can notice well resolved symmetric circular wave. As time evolves the wave propagates and is being reflected from the left boundary. The Mach steam which is evolving behind the main wave can be recognized in Figure 4. This problem can be considered as a model for a pointwise disturbance of a still water surface, e.g. as it occurs when a stone is thrown into a lake.

As mentioned above, we set reflected boundary conditions on the left vertical boundary and absorbing boundary conditions elsewhere. In numerical experiments presented in this paper we have implemented absorbing boundary conditions by linear extrapolation of all quantities to the so-called ghost cells, which are adjacent to the boundary of the computational domain. Thus, we have, e.g. for the pressure wave ϕ,

$$\phi_{-1j}=\phi_{0j},\ \phi_{-2j}=\phi_{1j},\quad j\in\mathbb{Z},$$

where Ω_{-1j}, Ω_{-2j} and Ω_{0j}, Ω_{1j} are the ghost cells and the cells belonging to Ω, respectively.

Note that due to the second order method two layers of the ghost cells are needed. The reflected boundary conditions are easily modelled by reflecting the interior data across the boundary and negating the normal component of velocity. Thus, we have on the left vertical boundary

$$u_{-1j}=-u_{0j},\ u_{-2j}=-u_{1j},\quad j\in\mathbb{Z}.$$

Other quantities, i.e. ϕ, v, are extrapolated.

5.3 Interaction between circular shocks and reflected waves

In this example we consider again the wave equation system (24) with the following discontinuous initial data

$$\begin{aligned}&\phi=1,\quad u=0,\quad v=0,\qquad \|\boldsymbol{x}\|<0.4\\&\phi=0,\quad u=0,\quad v=0,\qquad \text{else.}\end{aligned}$$

The computational domain $[-1,1]\times[-1,1]$ is divided into 200×200 cells. We implemented reflected boundary conditions on the vertical boundaries and absorbing boundary conditions on the horizontal ones. In Figure 5 the pressure wave distribution at different times $T=0.3,1.0,1.3$ is depicted. We can notice a well-resolved circular shock travelling away from the center of the computational domain. As time evolves the shock reaches the vertical boundaries and is reflected into the computational domain. Due to the linear model interactions between the linear circular shock and reflected waves can be observed very well.

5.4 Euler equations and cylindrical explosion

The third example is a two-dimensional circular Riemann problem for the nonlinear system of Euler equations with the initial data

$$\begin{aligned}&\rho=1,\quad u=0,\quad v=0,\quad p=1,\qquad \|\boldsymbol{x}\|<0.4\\&\rho=0.125,\quad u=0,\quad v=0,\quad p=0.1,\quad \text{else.}\end{aligned}$$

Figure 6 shows the density distribution as a function of x and y at different output times $T=0.0,\ 0.23,\ 0.38,\ 0.6,\ 1.3,\ 2.0$. The computational domain $[-1,1]\times[-1,1]$ is divided into 100×100 cells. As time evolves a complex wave pattern emerges. The solution exhibits a circular shock travelling away from the center, a circular contact discontinuity travelling in the same direction and a circular rarefaction wave travelling towards the origin at $(0,0)$. We have inserted absorbing boundary conditions on the whole $\partial\Omega$. This result illustrates good multidimensional resolution for long-time simulations and preservation of rotational symmetry of the numerical solution to nonlinear systems. Note that this example can be considered as a benchmark problem for the entropy fix. In fact we need no special treatment in order to resolve the sonic rarefaction wave correctly, see also [12] for further experiments confirming this point.

References

1. T.J. Barth, D.C. Jespersen, The design and application of upwind shemes on unstructered meshes, AIAA paper **336**, (1989).
2. M. Brio, A.R. Zakharian, G.M. Webb, Two-dimensional Riemann solver for Euler equations of gas dynamics, J. Comput. Phys.**167(1)**, (2001) 177-195.
3. M. Fey, Multidimensional upwinding, Part II. Decomposition of the Euler equations into advection equations, J. Comp. Phys. **143**, (1998) 181-199.
4. A. Kurganov, S. Noelle, G. Petrova, Semidiscrete central-unpwind schemes for hyperbolic conservation laws and Hamilton-Jacobi equations, SIAM J. Sci. Comput. **23(3)**, (2001) 707-740.
5. R.J. LeVeque, Wave propagation algorithms for multi-dimensional hyperbolic systems, J. Comp. Phys. **131**, (1997) 327-353.
6. J. Li, M. Lukáčová-Medviďová, G.Warnecke, Evolution Galerkin schemes for the two-dimensional Riemman problems, Discrete and Continuous Dynamical Systems (A), **9(3)**, (2003) 559–578.
7. M. Lukáčová - Medviďová, K.W. Morton, G. Warnecke, Evolution Galerkin methods for hyperbolic systems in two space dimensions, MathComp. **69**, (2000) 1355–1384.
8. M. Lukáčová - Medviďová, K.W. Morton, G. Warnecke, High-resolution finite volume evolution Galerkin schemes for multidimensional hyperbolic conservation laws, *Numerical Mathematics and Advanced Applications* (eds. Neittaanmäki, Pekka et al.), World Scientific Publishing Company, Singapore, (2000) 633–640.

9. M. Lukáčová-Medviďová, K.W. Morton, G. Warnecke. Finite volume evolution Galerkin methods for Euler equations of gas dynamics, Int. J. Numer. Meth. Fluids **40**, (2002) 425-434.
10. M. Lukáčová-Medviďová, K.W. Morton, G. Warnecke. Finite volume evolution Galerkin (FVEG) methods for hyperbolic problems, *submitted to SISC*.
11. M. Lukáčová - Medviďová, G. Warnecke, Lax-Wendroff type second order evolution Galerkin methods for multidimesnional hyperbolic systems, East-West Journal **8(2)**, (2000) 127–152.
12. M. Lukáčová - Medviďová, J. Saibertová, G. Warnecke, Finite volume evolution Galerkin methods for nonlinear hyperbolic systems, J. Comp. Phys. **183**, (2002) 533–562.
13. M. Lukáčová - Medviďová, G. Warnecke, Y. Zahaykah, Third order finite volume evolution Galerkin (FVEG) methods for two-dimensional wave equation system, submitted to East-West J. Numer. Anal. (2002).
14. M. Lukáčová - Medviďová, G. Warnecke, Y. Zahaykah, On the boundary conditions for EG-methods applied to the two-dimensional wave equation systems, submitted to ZAMM (2002).
15. K.W. Morton, On the analysis of finite volume methods for evolutionary problems, SIAM J. Numer. Anal. **35(6)**, (1998) 2195-2222.
16. K.W. Morton, Discretisation of unsteady hyperbolic conservation laws, SIAM J. Numer. Anal. **39(5)**, (2001) 1556-1597.
17. S. Noelle, The MOT-ICE: a new high-resolution wave-propagation algorithm for multi-dimensional systems of conservative laws based on Fey's method of transport, J. Comput. Phys. **164**, (2000) 283–334.
18. S. Ostkamp, Multidimensional characterisitic Galerkin schemes and evolution operators for hyperbolic systems, Math. Meth. Appl. Sci. **20**, (1997) 1111-1125.
19. S. Ostkamp, *Multidimensional characteristic Galerkin schemes and evolution operators for hyperbolic systems*, PhD thesis (University Hannover, 1995).
20. Y. Zahaykah, *Evolution Galerkin schemes and discrete boundary conditions for multidimensional first order systems*, PhD thesis (University of Magdeburg, 2002).

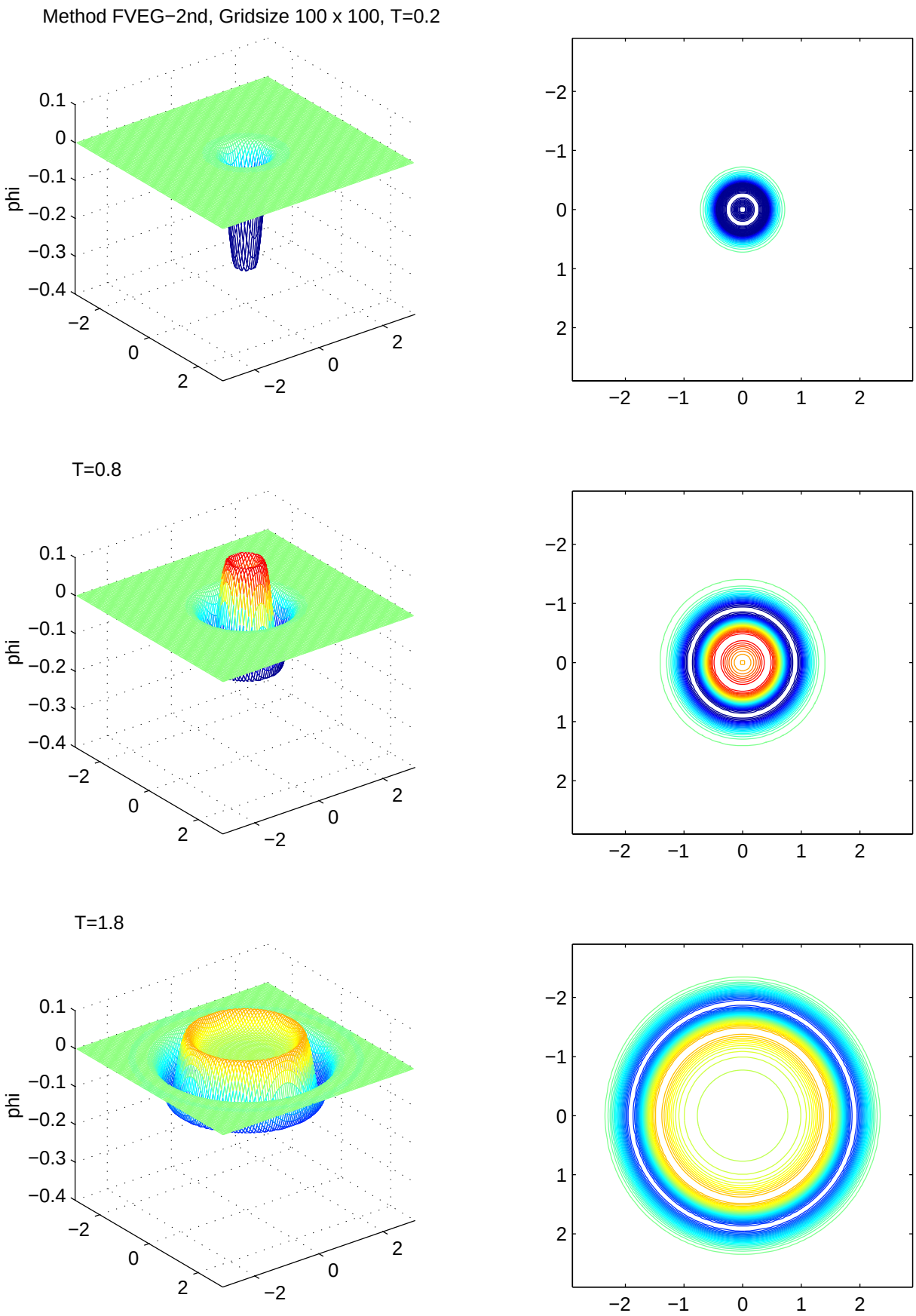

Fig. 2. Propagation of circular water waves

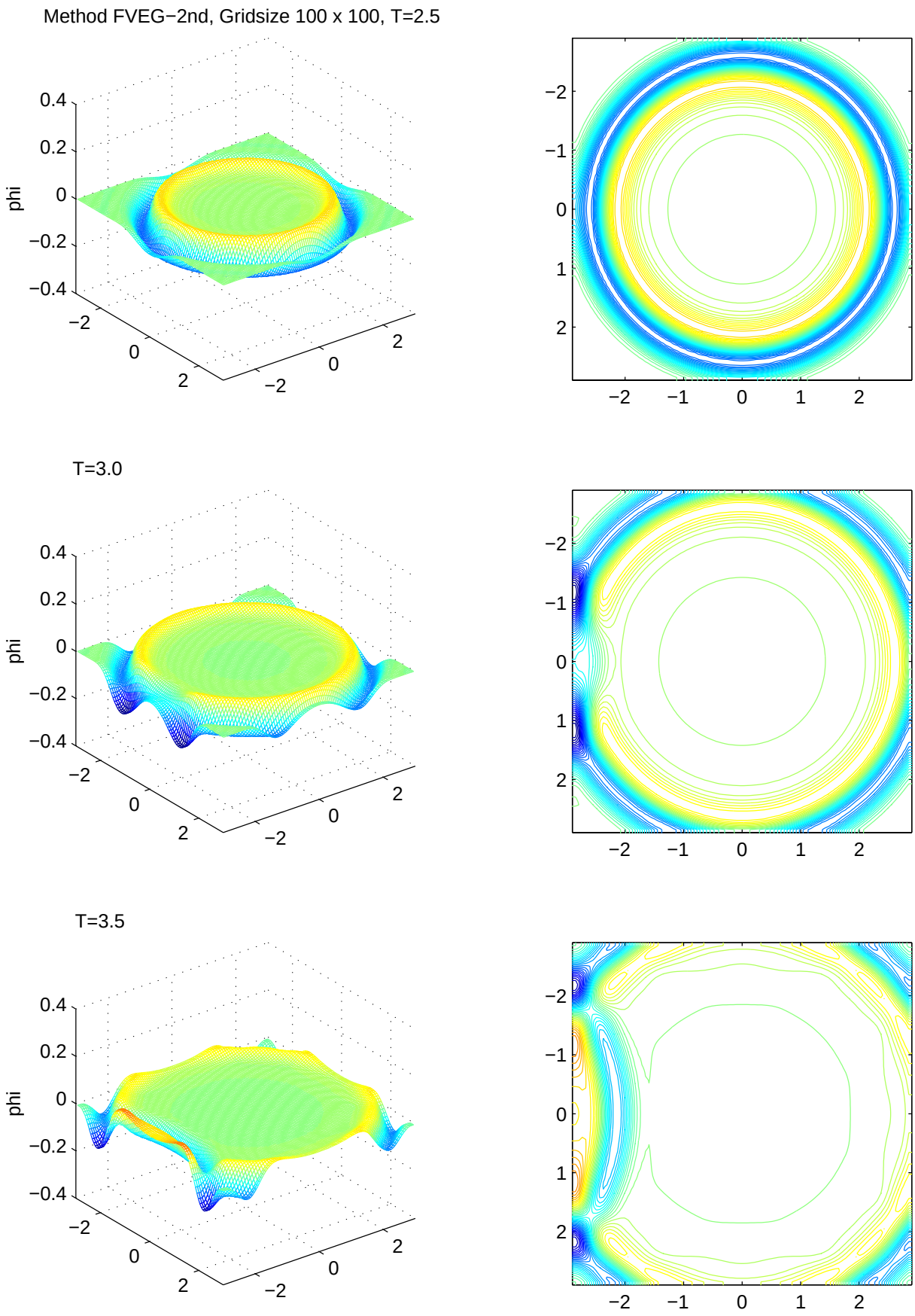

Fig. 3. Propagation of circular water waves (continues)

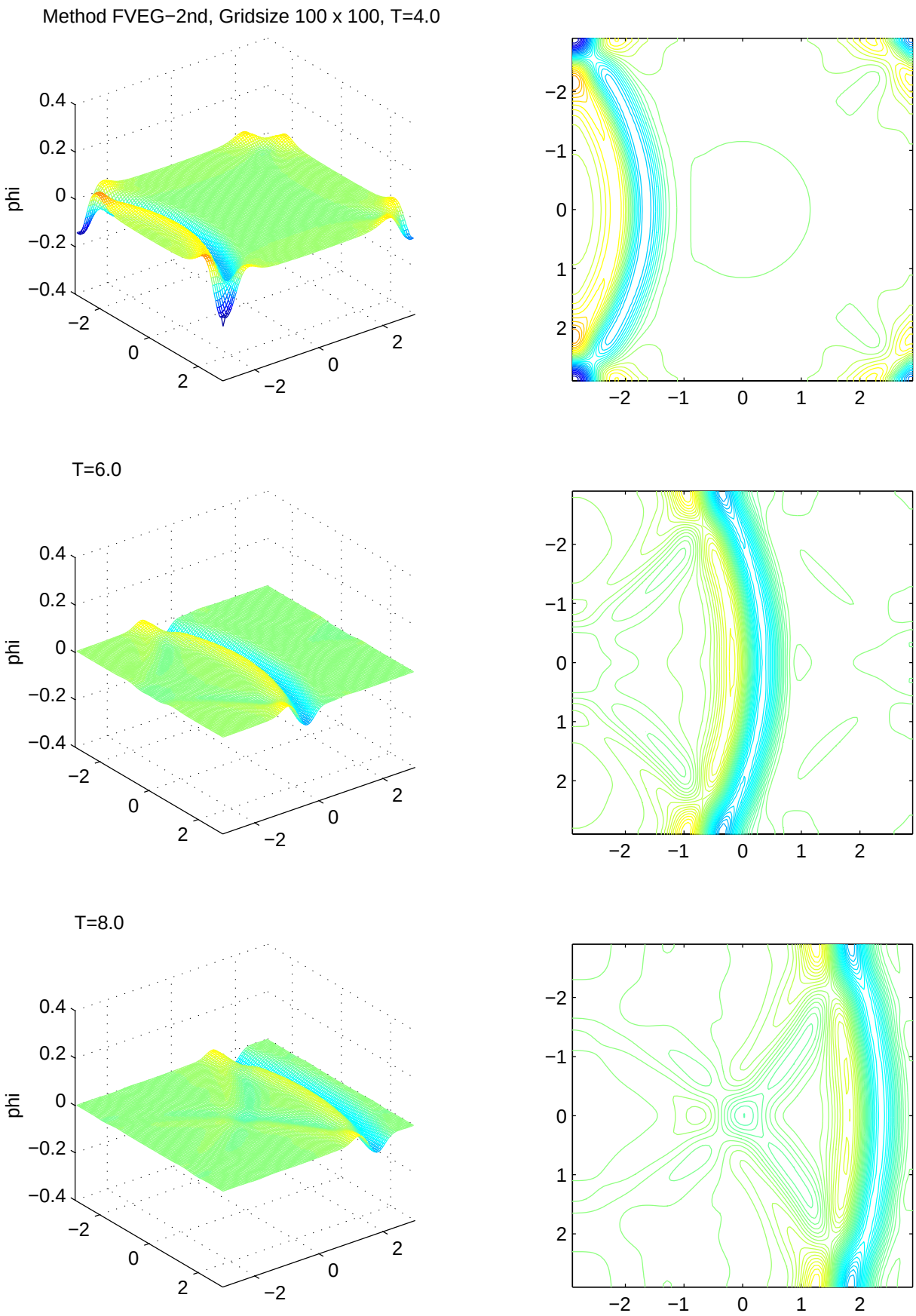

Fig. 4. Propagation of circular water waves (finished)

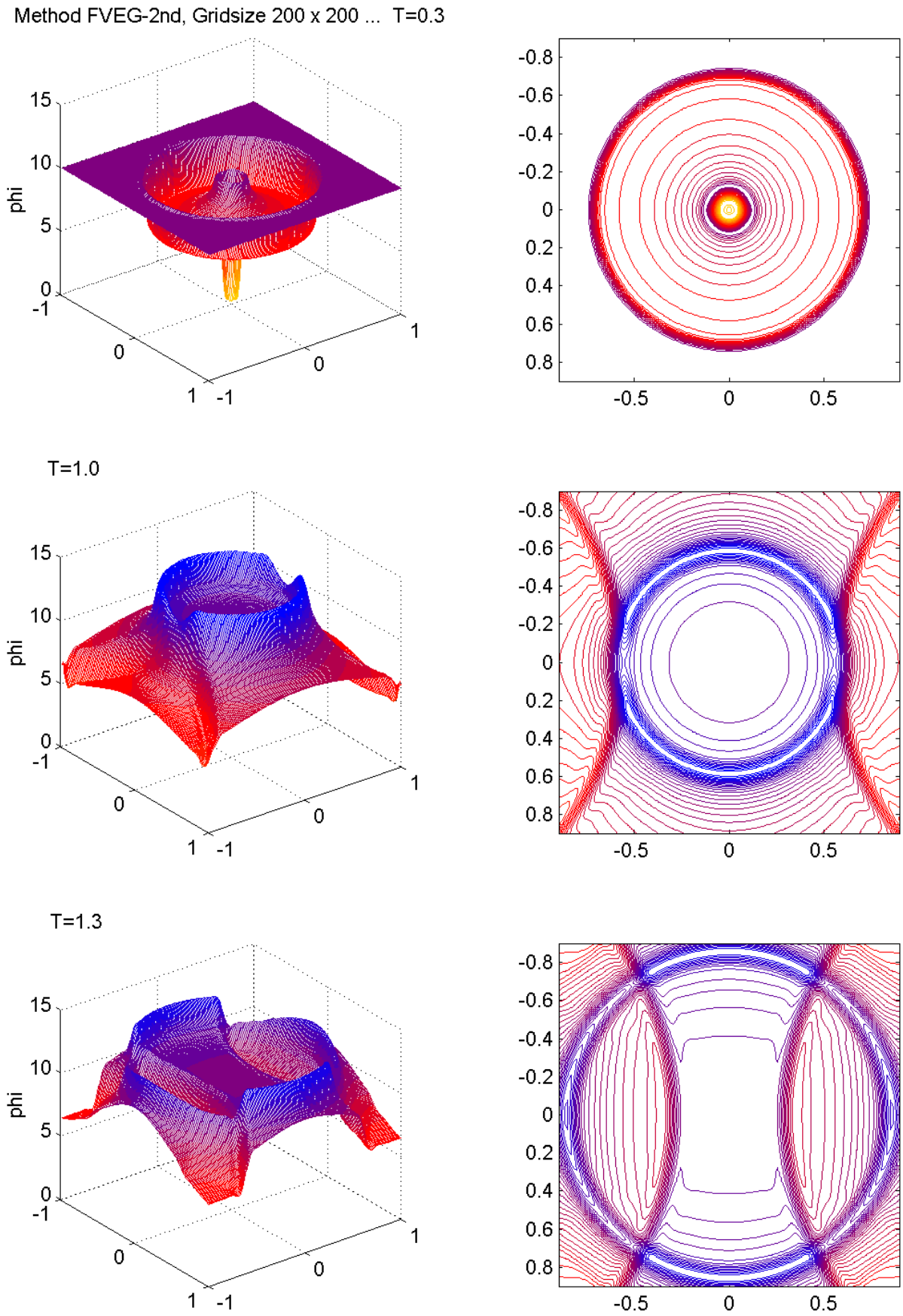

Fig. 5. Interaction between the circular shock and reflected waves

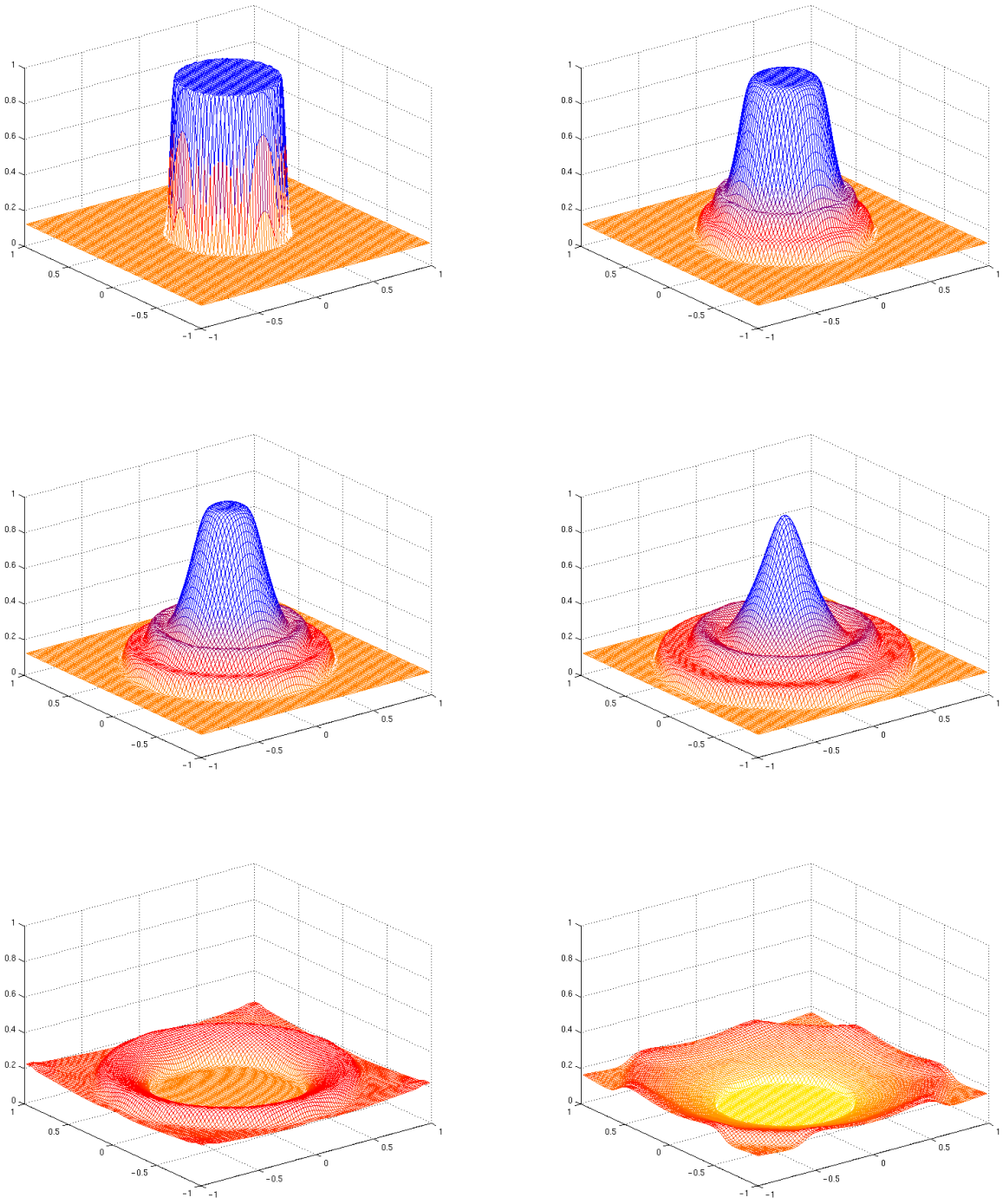

Fig. 6. Density distribution of cylindrical explosion problem at $T = 0.0$ (above left), $T = 0.23$ (above right), $T = 0.38$ (middle left), $T = 0.6$ (middle right), $T = 1.3$ (below left), $T = 2.0$ (below right).